Photoacoustics 35 (2024) 100583

Contents lists available at ScienceDirect

Photoacoustics

journal homepage: www.elsevier.com/locate/pacs

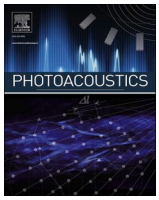

High sensitivity and ultra-low concentration range photoacoustic spectroscopy based on trapezoid compound ellipsoid resonant photoacoustic cell and partial least square

Qiaoyun Wang [a,b,*], Shunyuan Xu [a], Ziheng Zhu [a], Jilong Wang [a], Xin Zou [a], Chu Zhang [c], Qiang Liu [a,b]

[a] College of Information Science and Engineering, Northeastern University, Shenyang, Liaoning Province 110819, China
[b] Hebei Key Laboratory of Micro-Nano Precision Optical Sensing and Measurement Technology, Qinhuangdao 066004, China
[c] National Key Laboratory of Science and Technology on Tunable Laser, Harbin Institute of Technology, Harbin 150001, China

ARTICLE INFO

Keywords:
Photoacoustic spectroscopy
Trace gas detection
Partial least square
Trapezoid compound ellipsoidal photoacoustic cell
C_2H_2 gas

ABSTRACT

A high sensitivity and ultra-low concentration range photoacoustic spectroscopy (PAS) gas detection system, which was based on a novel trapezoid compound ellipsoid resonant photoacoustic cell (TCER-PAC) and partial least square (PLS), was proposed to detect acetylene (C_2H_2) gas. In the concentration range of 0.5 ppm ~ 10.0 ppm, the limit of detection (LOD) values of TCER-PAC-based PAS system without data processing was 66.4 ppb, which was lower than that of the traditional trapezoid compound cylindrical resonant photoacoustic cell (TCCR-PAC). The experimental results indicated that the TCER-PAC had higher sensitivity than of TCCR-PAC. Within the concentration range of 12.5 ppb ~ 125.0 ppb, the LOD and limit of quantification (LOQ) of TCER-PAC-based PAS system combined with PLS regression algorithm were 1.1 ppb and 3.7 ppb, respectively. The results showed that higher detection sensitivity and lower LOD were obtained by PAS system with TCER-PAC and PLS than that of TCCR-PAC-based PAS system.

1. Introduction

Oil-immersed transformers are the most important parts of power systems. Transformer failures will affect the industrial production and human life. Acetylene (C_2H_2) is generally regarded as the characteristic gas of oil-immersed transformer. The concentration of C_2H_2 dissolved in oil could be used to judge the faults of transformer, such as overheating and discharge failures [1–3]. The C_2H_2 concentration in the dissolved oil is generally below ppm. Therefore, in order to realize the early faults detection of the oil-immersed transformer, the method to detect C_2H_2 with high accuracy and sensitivity is demanded. There are many methods to detect C_2H_2 gas, such as electrochemistry method, semiconductor method, and catalyst combustion methods, but the disadvantages of these conventional methods are high price, difficult maintenance, poor stability, low selectivity and sensitivity [4]. Laser spectroscopy-based gas sensing approach has advantages of non-contact measurement and fast response [5–10]. Photoacoustic spectroscopy (PAS) is an important optical method to detect the trace gas due to its high sensitivity and excellent selectivity [11–21].

Over the last decade, researchers have mainly enhance performance of PAS through three types of techniques: (1) Optimizing the photoacoustic cell (PAC) structure, such as replacing the cylindrical resonance cavity with an ellipsoid, amplifying the number of resonance cavities to create a differential cell structure, modifying the buffer cavity to a step-type, or diminishing the number of buffer cavities by one, resulting in a shift from H-type to T-type designs [11–15,22]. (2) Using microphone with high sensitivity, such as silicon cantilever beam optical fiber microphones or high-quality quartz tuning forks, which are better choose for detecting and enhancing the performance of the PAS [23–25]. (3) Increasing the optical path length (OPL) or incident light power, such as the concave reflector mirrors or other type mirrors are used to increase the OPL by multiple reflections of laser in the PAC [26]. Installing multiple incident light on the same or opposite side are used to increase the power of laser [15,16,27–31].

Many works on the structural optimization of PACs have been reported [12–15,32,33]. Zha *et al.* designed a resonant cavity in the T shape with a wide top and narrow bottom [32]. Instead of the typical conventional PAC, Liu *et al.* used a miniaturized T-type PAC composed

* Corresponding author at: College of Information Science and Engineering, Northeastern University, Shenyang, Liaoning Province 110819, China.
E-mail address: wangqiaoyun@neuq.edu.cn (Q. Wang).

https://doi.org/10.1016/j.pacs.2023.100583
Received 3 November 2023; Received in revised form 26 December 2023; Accepted 27 December 2023
Available online 30 December 2023

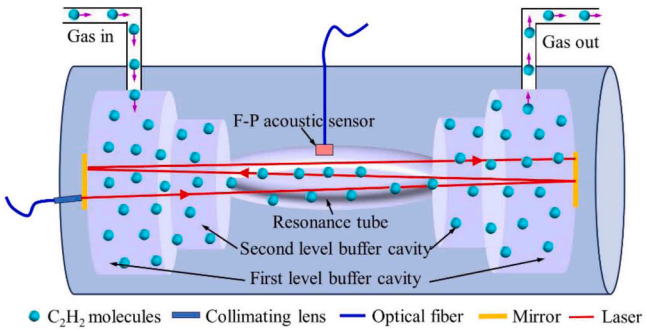

Fig. 1. The schematic structure of designed TCER- PAC. The length of the resonance tube was 100 mm. And the radiuses of the semi-major axis and semi-minor axis of the resonator tube were 60 mm and 4 mm, respectively. The length of the first level and the second level buffer volume on both sides were both 25 mm. The diameters of the first level and the second level buffer volume were 35 mm and 17.5 mm, respectively.

by a horizontal absorber cavity, vertical buffer and resonance cavity to quantitatively analyze the environmental pollutants [33]. Gong *et al.* presented a T-type half-open resonant PAC with a single buffer volume for C_2H_2 gas detection [34]. The H-type longitudinal resonant PAC with radius of 2 mm and length of 120 mm was optimized by Gong *et al.* for NO_2 gas detection [29]. In 2021, Gong *et al.* reported a spherical integrated PAC [35]. Furthermore, an ellipsoidal resonant PAC was proposed by Wang *et al.*, which was compared with the H-type PAC [36]. The experimental results showed that the signal-to-noise of ellipsoid PAC was better than that of cylindrical PAC. However, the impact of the airflow and vortex backflow on PAC was not considered. A trapezoid compound H-type PAC was presented and analyzed by Cheng *et al.*, the results shown that the velocity gradient in the trapezoidal composite PAC cavity will become more stable, and the impact of gas vortex return to the cavity was reduced [37].

To get the combination of high sensitivity and ultra-low concentration detection, a PAS sensor with trapezoid compound ellipsoid resonant photoacoustic cell (TCER-PAC) and the partial least square (PLS) regression algorithm was proposed in this paper. The finite element model was built to simulate the acoustic properties of the novel PAC using COMSOL Multiphysics. The resonance frequency and acoustic pressure distribution on the performance of PAS were discussed. According to the simulation results, the PA signal of TCER-PAC-based PAS system was stronger than that of trapezoid compound cylindrical resonant photoacoustic cell (TCCR-PAC)-based PAS system. With data processing, the limit of detection (LOD) value and limit of quantification (LOQ) value have been reached the ppb level. In our experiments, the PAS sensor with TCER-PAC and data processing can be used to detect C_2H_2 trace gas with high sensitivity and ultra-low detection limit.

2. System design

2.1. PAC design

The TCER-PAC was designed as shown in Fig. 1. The trapezoidal buffer cavity was composed by an ellipsoidal resonance tube and two cylindrical buffer cavities with different diameters. The PA signal of TCER-PAC would be increased with the cavity length [34]. The COMSOL software was used to establish a TCER-PAC model. In the meshing process, the element size was 0.5 mm ~ 0.8 mm with 1.3 growth rate. The length of the first level and the second level buffer cavities were both 25 mm, and the diameters of the first level and the second level buffer volume were 35 mm and 17.5 mm, respectively. The length of the ellipsoidal resonance tube was 100 mm, and the diameters of semi-major axis and semi-minor axis were 60 mm and 4 mm, respectively.

The frequency response and acoustic field characteristics of TCER-PAC were simulated and solved, as shown in Fig. 2 and Fig. 3. The resonance frequency of TCER-PAC was 1300 Hz in Fig. 2, which was lower than the resonance frequency of 1580 Hz for the TCCR-PAC. The lower resonance frequency, the easier to demodulate the Fabry-Perot (F-P) acoustic sensor. The acoustic pressure distribution of the TCER-PAC and TCCR-PAC were shown in Fig. 3. The maximum acoustic pressure in the middle of TCER-PAC was 5.25×10^{-5} Pa with the 1300 Hz, which was two times than that of TCCR-PAC. The simulation results proved that TCER-PAC has a better performance than the TCCR-PAC.

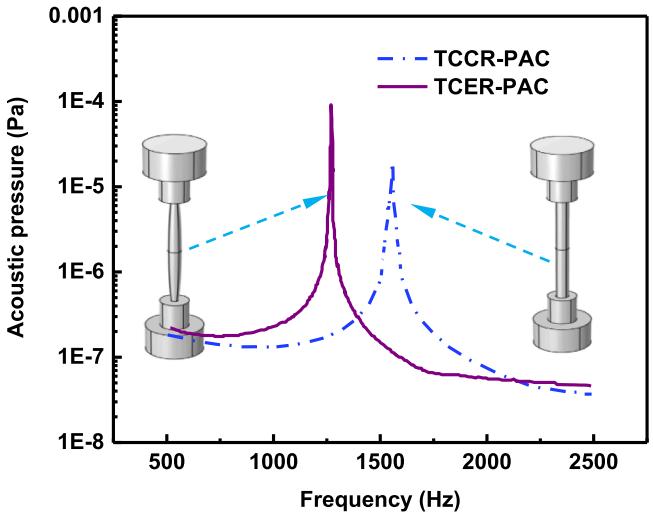

Fig. 2. The simulated frequency responses of the TCER-PAC and TCCR-PAC. The resonance frequency of TCER-PAC and TCCR-PAC were 1300 Hz and 1580 Hz, respectively. (In the meshing process, the heat source domain feature was used to replace the heat, and the element size was 0.5 mm ~ 0.8 mm with 1.3 growth rate.).

2.2. PA system design

C_2H_2 had a strong absorption at 1532.83 nm. In our experimental, the distributed feedback lasers (DFB) laser with modulated wavelength range 1532.75 nm ~ 1532.85 nm was used as the excitation light. Firstly, the wavelength of DFB laser was modulated with sawtooth and sine waves of different frequencies. Then, an erbium-doped fiber amplifier (EDFA) was used to amplify the optical power of wavelength-modulated laser. Finally, the amplified laser was input into the PAC through the collimator. The Fabry-Perrot optical fiber sensor [38] was used to detect the PA signal. The diagram of the C_2H_2 PAS system was shown in Fig. 4.

2.3. Data processing

The peak of 2 f signal was proportional to C_2H_2 concentration is below 125.0 ppb. When the C_2H_2 concentration was below 62.5 ppb, the peak of 2 f signal was submerged in the noise and cannot be obtained directly. In this paper, the data analysis methods in chemometrics were firstly investigated. The pre-processing methods were used to reduce the effects of the noise and irrelevant information in the 2 f signal. The influence of spectral variability can be eliminated by the direct orthogonal signal correction algorithm (DOSC) [36]. Savitzky-Golay (SG) filters and the baseline correction were used for spectral smoothing and elimination of baseline shifts, respectively. After the pre-processing, the relationship between the C_2H_2 concentration and 2 f signal was established by PLS [37]. At first, the C_2H_2 concentration and 2 f signal were projected onto a latent space using PLS and the maximizes correlation between them can be obtained. Then, the best match function can be found by minimizing the sum of squares of errors, and a regression model can be built. At last, the C_2H_2 concentration can be predicted by the 2 f

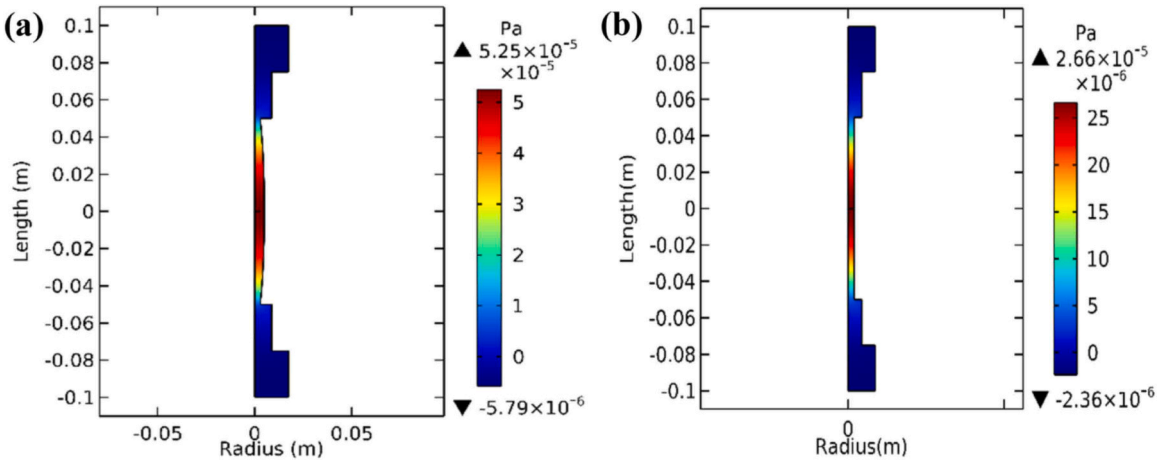

Fig. 3. The simulation results of the acoustic pressure distribution of the (a) TCER-PAC and (b) TCCR-PAC. The maximum acoustic pressure in the middle of TCER-PAC and TCCR-PAC were 5.25 × 10^{-5} Pa at 1300 Hz and 2.66 × 10^{-5} Pa at 1580 Hz, respectively. (In the meshing process, the heat source domain feature was used to replace the heat, and the element size was 0.5 mm ~ 0.8 mm with 1.3 growth rate.).

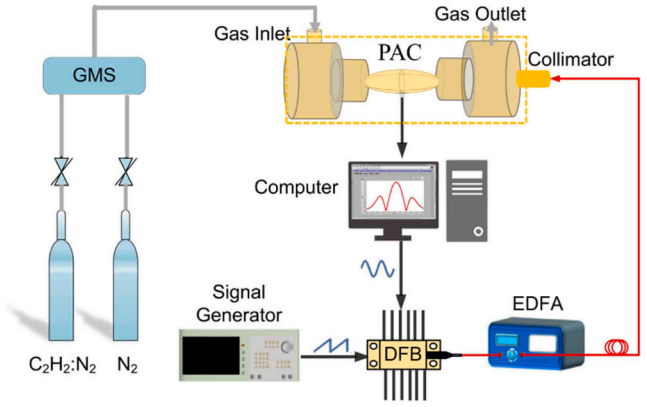

Fig. 4. Schematic diagram of the C_2H_2 PAS system. EDFA, erbium-doped fiber amplifier; GMS, gas mixture system; DFB, distributed feedback lasers, the wavelength was modulated from 1532.75 nm to 1532.85 nm. The path of the laser beam was labeled by red lines. The path of electrical signal was marked as black lines. The gray lines were used to show the transmission of gas. The PAC is the same structure as that shown in Fig. 1.

signal. In common words, the parameters of PLS model were firstly obtained by the 2 *f* signals with known concentration, and then the established PLS model was used to predicted the concentration corresponding to the 2 *f* signal with known concentration. At last, the predicted concentration was compared with the known concentration to obtain the relationship between them. The coefficient of determination (R^2) [38] is used to evaluate the relationship between the concentration of C_2H_2 trace gas and 2 *f* signal. There is a better fitness and prediction performance of the PLS model when the R^2 is closer to 1. The residual predictive deviation of prediction (RPD) was used to indicate the precision of PLS model. When the value of RPD was larger than 3, the predictive performance of PLS model was considered excellent. The root mean squared error (RMSE) was used to represent the PLS model performance in the calibration step (RMSEC) and prediction step (RMSEP) [39–42]. The smallest values of RMSEC and RMSEP, the quantitative performances of the model were best [43]. The definition of R^2, RPD, RMSEC and RMSEP were calculated as:

$$R^2 = 1 - \frac{\sum_{i=1}^{N_c} (\hat{y}_{i,c} - y_{i,c})^2}{\sum_{i=1}^{N_c} (\bar{y}_c - y_{i,c})^2} \quad (1)$$

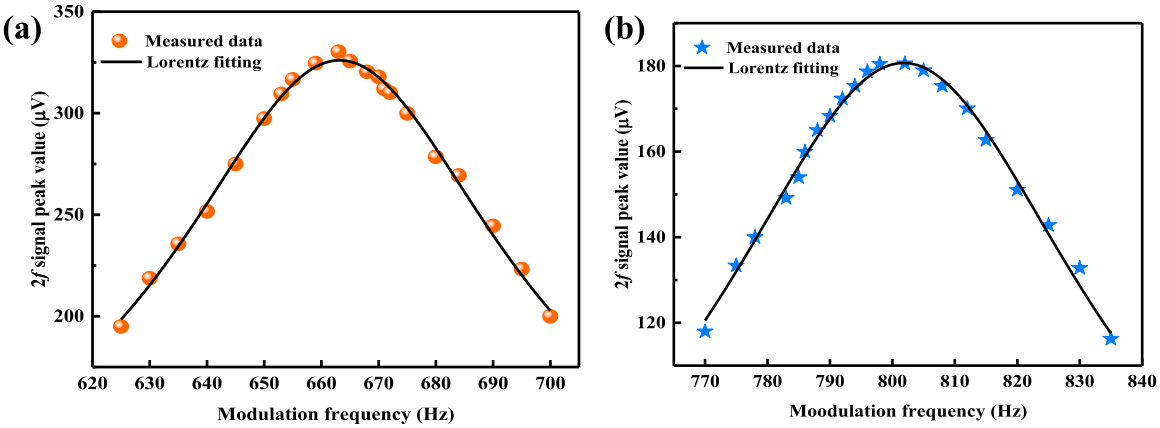

Fig. 5. Frequency responses of the (a) TCER-PAC and (b) TCCR-PAC. The amplitude of the 2 *f* signal measured for 10.0 ppm C_2H_2:N_2. The wavelength of DFB was modulated from 1532.75 nm ~ 1532.85 nm. The power of the DFB laser was amplified to 200 mW. The 2 *f* signal of TCER-PAC-based PAS system reached its maximum value when the modulation frequency was 663 Hz and the peak of 2 f signal peak of TCCR-PAC was at 798 Hz.

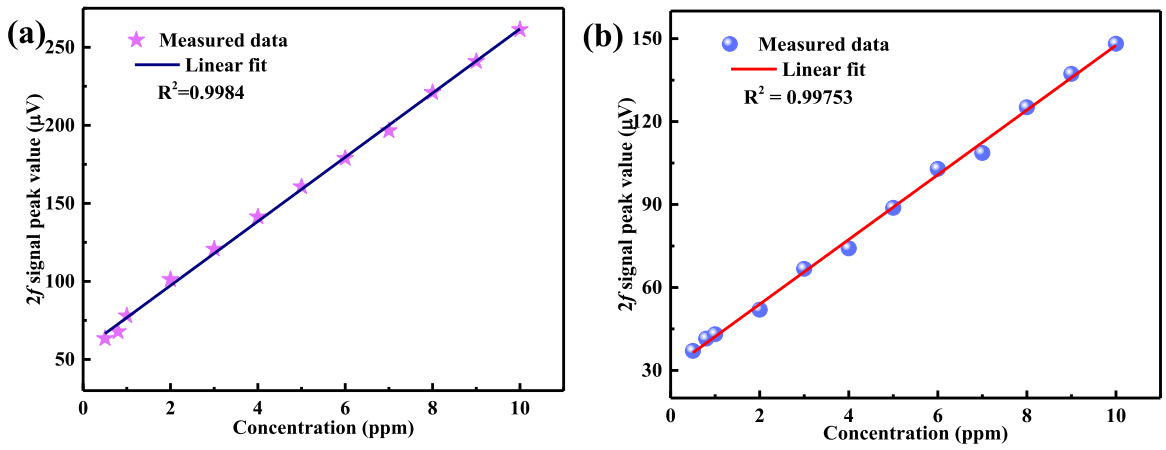

Fig. 6. Measurement result and fitting curve of (a) the TCER-PAC and (b) the TCCR-PAC. The 2 *f* signal peak value of each concentration was continuously measured for 5 min with the sampling interval 1 s. The incident power was 200 mW. All these experiments were performed under room temperature and atmospheric pressure.

$$RPD = \sqrt{\frac{\sum_{i=1}^{N_p}(\bar{y}_p - y_{i,p})^2}{\sum_{i=1}^{N_p}(\hat{y}_{i,p} - y_{i,p})^2}} \tag{2}$$

$$RMSEC = \sqrt{\frac{\sum_{i=1}^{N_c}(\hat{y}_{i,c} - y_{i,c})^2}{N_c}} \tag{3}$$

$$RMSEP = \sqrt{\frac{\sum_{i=1}^{N_p}(\hat{y}_{i,p} - y_{i,p})^2}{N_p}} \tag{4}$$

where N_c and N_p were represented the number of samples in the calibration and prediction respectively; $y_{i,c}$ and $y_{i,p}$ were the reference concentration of samples in the calibration set and prediction set respectively; $\hat{y}_{i,c}$ and$\hat{y}_{i,p}$ were the predicted concentration of the calibration set and prediction set respectively; $\bar{y}_c$ and $\bar{y}_p$ were the average concentration of the calibration set and prediction set respectively.

The limit of detection (LOD) was the ability to detect the minimum concentration and the limit of quantification (LOQ) was used to represent the accurate measurement ability of samples with known concentration. For the PLS regression model, the LOD and LOQ can be obtained from the standard deviation (SD, S_a) of the model and the slope of the regression curve (b), as shown below [44–47]:

$$LOD = 3 \times S_a/b \tag{5}$$

$$LOQ = 10 \times S_a/b \tag{6}$$

For the linear regression, the S_a can be estimated by the y-residuals or y-intercepts of the regression lines. In this paper, the S_a was the standard deviation of y-intercepts of regression lines.

3. Experimental results and discussion

The PA signal intensities with different modulated frequency of TCER-PAC-based PAS system and TCCR-PAC-based PAS system were shown in Fig. 5 **(a)** and **(b)**, respectively. As shown in Fig. 5 **(a)**, the 2 *f* signal peak of TCER-PAC-based PAS system reached its maximum value when the modulation frequency was 663 Hz. And the resonance frequency of TCER-PAC-based PAS system was 1326 Hz, which was similar to the simulation result of 1300 Hz. In Fig. 5 **(b)**, the modulation frequency was 798 Hz when the 2 *f* signal peak of TCCR-PAC-based PAS system reached the maximum value. The resonance frequency of TCCR-PAC-based PAS system was 1596 Hz, which was similar to the simulation results of 1580 Hz. In our experiment, the laser modulation frequencies of the TCER-PAC-based PAS system and TCCR-PAC-based PAS system were 663 Hz and 798 Hz, respectively.

The C_2H_2:N_2 concentration was controlled by two mass flow

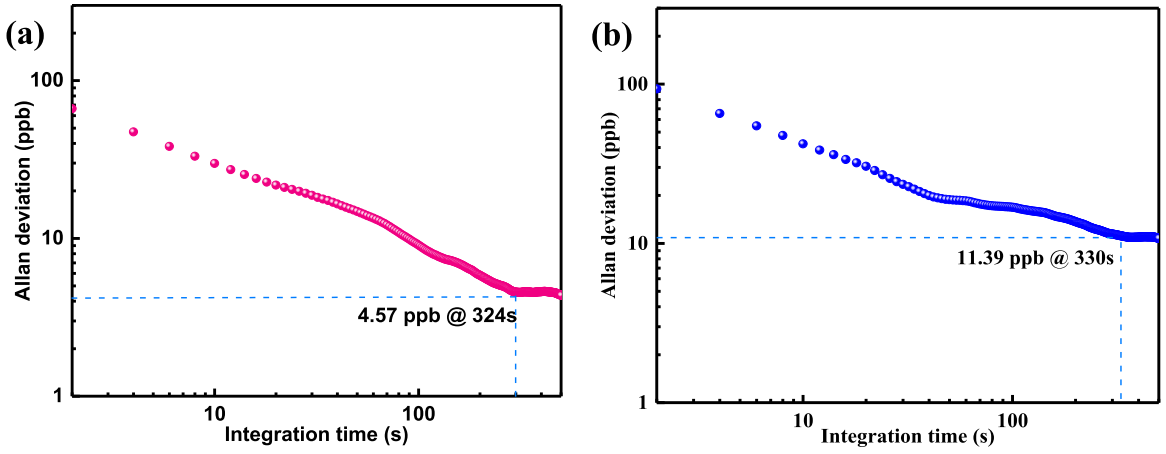

Fig. 7. Allan deviation of the (a) TCER-PAC and (b) TCCR-PAC. The 2 *f* signal peak value was measured for an hour with a sampling interval of 1 s. The wavelength of DFB was modulated from 1532.75 nm ~ 1532.85 nm. The incident power was 200 mW. All these experiments were performed under room temperature and atmospheric pressure.

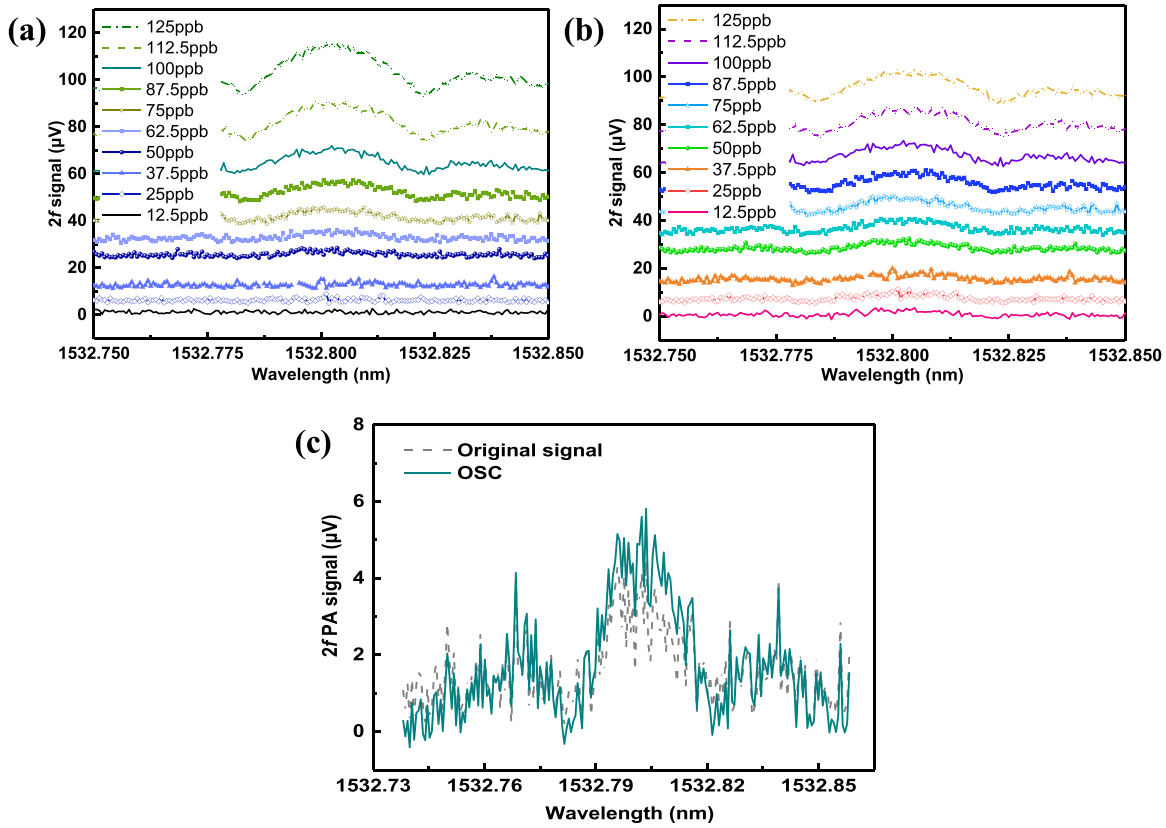

Fig. 8. 2 *f* signal of C_2H_2 gas for an incident optical power of 200 mW (a) without pre-processing. (b) with OSC pre-processing. The concentration of C_2H_2 was varied from 12.5 ppb to 125.0 ppb. (c) the comparison between the original signal and the signal with DOSC preprocessing when the concentration of C_2H_2 gas was 0.05 ppm. And the 2 *f* signal peak value of each concentration was continuously measured for 5 min with the sampling interval 1 s.

controllers, one mass flow meter was used to control the flow of pure N_2 gas and the other was used to control the flow of C_2H_2:N_2 gas mixture (the concentration of C_2H_2 is 10.0 ppm). According to the 2 *f* signal detection method, the modulation frequencies of the laser were set at 663 Hz in TCER-PAC-based PAS system and 798 Hz in TCCR-PAC-based PAS system, respectively. The each 2 *f* signal was continuously measured for 5 min with the sampling interval 1 s. The relationship between 2 *f* signal peak value and C_2H_2 concentration was shown in Fig. 6. In the concentration range of 0.5 ppm ~ 10.0 ppm, there was a good linear relationship between the 2 *f* signal peak value and C_2H_2 concentration. The linear equation was expressed as:

$$2f\text{PeakValue}(\mu\text{V}) = a \times C(\text{ppm}) + b \quad (7)$$

where C was the concentration of C_2H_2 gas, a and b were the slope and intercept of the fit line, respectively.

In Fig. 6 **(a)**, the parameter values in the linear equation of the TCER-PAC-based PAS system were $a = 20.6 \pm 0.3$ μV/ppm and $b = 56.1 \pm 1.5$ μV, respectively. In Fig. 6 **(b)**, the parameter values in the linear fitting equation of the TCCR-PAC-based PAS system were $a = 11.5 \pm 1.1$ μV/ppm and $b = 30.9 \pm 6.1$ μV, respectively. Experimental results showed that the sensitivity of was 2 times that of TCCR-PAC-based PAS system.

The 2 *f* signals of PAS system with pure N_2 were continuously measure for 60 min and analyzed as background noise of PAS system. The Allan deviations calculated results of the TCER-PAC-based PAS system and TCCR-PAC-based PAS system were obtained, as shown in Fig. 7. The LOD of TCER-PAC-based PAS system is 66.4 ppb at integration time of 1 s. And the LODs were 4.6 ppb at 324 s integration time. When the integration times were 1 s and 330 s, the LOD the TCCR-PAC-based PAS system were 93.4 ppb and 11.4 ppb, respectively. From the experimental results, the LOD of TCER-PAC-based PAS system is 30% lower than that of TCCR-PAC-based PAS system. The normalized noise equivalent absorption (NNEA) coefficient of the TCER-PAC-based PAS system was 2.2×10^{-8} $cm^{-1}\bullet W\bullet Hz^{-(1/2)}$, which is lower than of 3.1×10^{-8} $cm^{-1}\bullet W\bullet Hz^{-(1/2)}$ of TCCR-PAC-based PAS system. The experimental results confirmed that the sensitivity of TCER-PAC-based PAS system was about 1.5 times higher than that of the TCCR-PAC-based PAS system. It was verified that the TCER-PAC structure can improve the sensitivity of the PAS system.

Table 1
The PLS regression results with different pre-processing.

Pre-processing	PLS	R^2	RPD	RMSEC (ppb)	RMSEP (ppb)
None	Yes	-0.1122	1.0	2.9	3.0
Normalization	Yes	0.8646	2.1	1.5	1.6
Continues wavelet transform	Yes	0.9463	2.2	1.4	1.2
Baseline correction	Yes	0.9535	2.8	1.1	1.2
Orthogonal signal correction	**Yes**	**0.9997**	**7.4**	**0.4**	**0.4**

When the C_2H_2 concentration was lower than 125.0 ppb, it was difficult to obtain the relationship between peak values of 2 *f* signal and C_2H_2 concentration without the data processing. The 2 *f* signal obtained when the concentrations of C_2H_2 gas were changed from 12.5 ppb to 125.0 ppb in 12.5 ppb intervals was shown in Fig. 8 **(a).** As shown in Fig. 8 **(a)**, the 2 *f* signal cannot be observed when the concentration of C_2H_2 was below 75 ppb. In order to realize ultra-low and high linearity measurement of C_2H_2, it was necessary to use the data preprocessing and linear regression method to analyze the *2 f* signal of PAS system. The preprocessing methods used in this paper were normalization, continues wavelet transform (CWT), baseline correction (BC) and orthogonal signal correction (OSC). After OSC preprocessing, the *2 f* signal was

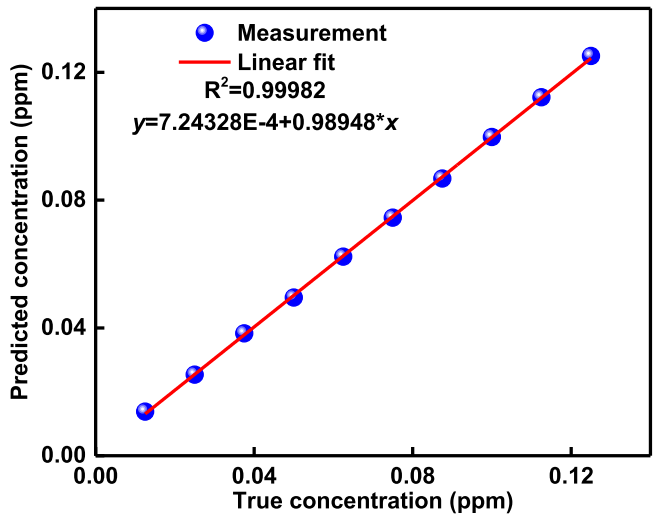

Fig. 9. Linear fitting of the predicted concentration and true concentration in 12.5 ppb ~ 125.0 ppb. The incident optical power was 200 mW.

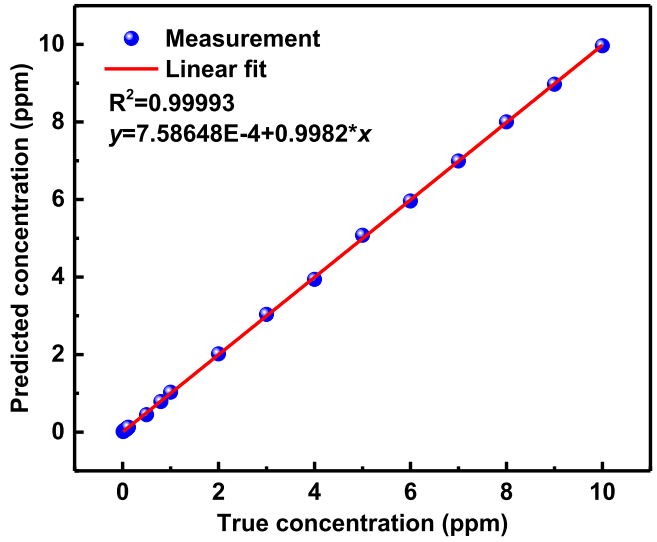

Fig. 10. Linear fitting of the predicted concentration and true concentration in 12.5 ppb ~ 10.0 ppm. The incident optical power was 200 mW.

show in Fig. 8 **(b)**. When the C_2H_2 concentration was 0.05 ppm, the comparison between the original signal and preprocessing signal was shown in Fig. 8 **(c)**. From visual inspection, the waveform preprocessed with OSC method can be better discerned than original signal. The comparison of the PLS model performance without and with preprocessing method was shown in Table 1. Without preprocessing, the linear relationship between the predicted and true concentration (R^2 =−0.1122) was bad. After preprocessing, the linearity of PLS model was greatly improved. The performance of PLS model established with OSC preprocessing method had the highest detection accuracy (R^2 =0.9997). Therefore, OSC was used to preprocess 2 *f* signals in subsequent experiments. Compared with other preprocessing methods, the OSC method was more suitable for analyzing *2 f* signal of PAS system. The analysis results of the principal component (PC) numbers in the PLS were shown in Fig. S1, Fig. S2 and Fig. S3.

The linear analysis result of PLS with OSC preprocessing was shown in Fig. 9. The predicted concentration is obtained by the PLS regression model. The linearity between the predicted concentration and the true concentration in 12.5 ppb ~ 125.0 ppb was obtained by the preprocessing and PLS method. In this paper, the relationship between the predicted concentration and the true concentration in 12.5 ppb ~ 10.0 ppm was shown in Fig. 10. The experimental results confirmed that the OSC preprocessing method was successful to exclude irrelevant information from original 2 *f* signal and PLS regression performed excellently in quantitative analysis of 2 *f* signals in PAS system.

Table 2
LOD and LOQ of PAS with PLS regression analysis.

Concentration range	R^2	S_a	*b*	LOD	LOQ
12.5 ppb ~125.0 ppb	0.9998	0.37	0.99	1.1	3.7

Table 3
Predicted C_2H_2 concentration with the PLS model.

Concentration	Test 1	Test 2	Test 3	Test 4	Test 5
12.5 ppb	14.3 ppb	14.2 ppb	14.0 ppb	13.8 ppb	13.5 ppb
125.0 ppb	124.0 ppb	126.7 ppb	125.0 ppb	126.1 ppb	125.8 ppb

According to the Eqs. (5) and (6), the LOD and LOQ of the TCER-PAC system with PLS regression can be given in the Table 2. In the range of 12.5 ppb ~ 125.0 ppb, the LOD after data processing was 1.1 ppb, which was lower than 66.4 ppb without data processing (Fig. 7).

Multiple experimental results have been analyzed through the PLS model, and the results were shown in Table 3. When the C_2H_2 concentration was 12.5 ppb, the mean was 14.0 ppb and SD was 0.3 ppb. When the C_2H_2 concentration of 125.0 ppb, the mean was 125.5 and SD was 1.0 ppb. When the concentration is ultra-low, the signal-to-noise ratio of 2 *f* signal was poor. The noise had a greater impact on the PLS predicted results. So, the predicted results deviated from the actual concentration. But the results show that the model still has good predictive ability for ultra-low concentrations.

4. Conclusion

In summary, an ultra-low and high sensitivity PAS system based on TCER-PAC and partial least square regression algorithm was proposed for C_2H_2 gas detection. The resonance frequency and acoustic signal intensity of TCER-PAC was simulated by COMSOL software. The simulation results indicated that the acoustic signal intensity of TCER-PAC structure was 1.5 times than that of TCCR-PAC. In the concentration range from 0.5 ppm to 10.0 ppm, the LOD of the TCER-PAC analyzed by Allan deviation was 66.4 ppb at integration time of 1 s, and 4.6 ppb at integration time of 324 s. The 2 *f* signal was analyzed by the OSC preprocessing and PLS regression algorithm when the C_2H_2 concentration was below 125.0 ppb, and the obtained of LOD and LOQ of from PLS model were 1.1 ppb and 3.7 ppb, respectively. The LOD was improved by about 60 times than that without PLS algorithm. The experimental results showed that a PAS system with TCER-PAC structure and PLS algorithm had a higher detection sensitivity and lower LOD than the TCCR-PAC without data processing. A new solution was provided for the high sensitivity and ultra-low concentration detection in this paper.

CRediT authorship contribution statement

Xu Shunyuan: Writing – review & editing, Software, Formal analysis. **Zhu Ziheng:** Writing – review & editing. **Wang Qiaoyun:** Writing – review & editing, Validation, Supervision, Software, Funding acquisition, Formal analysis, Conceptualization. **Zhang Chu:** Resources, Methodology. **Liu Qiang:** Writing – review & editing. **Wang Jilong:** Validation. **Zou Xin:** Software.

Declaration of Competing Interest

The authors declare that they have no known competing financial

interests or personal relationships that could have appeared to influence the work reported in this paper.

Data availability

Data will be made available on request.

Acknowledgment

This work was supported by the National Natural Science Foundation of China (NFSC 11404054, 61601104), the Natural Science Foundation of Hebei Province (F2019501025, F2020501040), the Fundamental Research Funds for the Central Universities (2023FZD002).

Appendix A. Supporting information

Supplementary data associated with this article can be found in the online version at doi:10.1016/j.pacs.2023.100583.

References

[1] L. Liu, H. Huan, W. Li, A. Mandelis, Y. Wang, L. Zhang, X. Zhang, X. Yin, Y. Wu, X. Shao, Highly sensitive broadband differential infrared photoacoustic spectroscopy with wavelet denoising algorithm for trace gas detection, Photoacoustics 21 (2021) 100228.
[2] M. Dong, C. Zheng, D. Yao, G. Zhong, S. Miao, W. Ye, Y. Wang, F.K. Tittel, Double-range near-infrared acetylene detection using a dual spot-ring Herriott cell (DSR-HC), Opt. Express 26 (9) (2018) 12081–12091.
[3] C. Zhang, S. Qiao, Y. He, S. Zhou, L. Qi, Y. Ma, Differential quartz-enhanced photoacoustic spectroscopy, Appl. Phys. Lett. 122 (24) (2023) 241103.
[4] L. Zhang, L. Liu, X. Zhang, X. Yin, H. Huan, H. Liu, X. Zhao, Y. Ma, X. Shao, T-type cell mediated photoacoustic spectroscopy for simultaneous detection of multi-component gases based on triple resonance modality, Photoacoustics 31 (2023) 100492.
[5] K. Hashimoto, T. Nakamura, T. Kageyama, V.R. Badarla, H. Shimada, R. Horisaki, T. Ideguchi, Upconversion Time-stretch Infrared Spectrosc., Light.: Sci. Appl. 12 (1) (2023) 48.
[6] X. Liu, Y. Ma, New temperature measurement method based on light-induced thermoelastic spectroscopy, Opt. Lett. 48 (21) (2023) 5687–5690.
[7] Z. Zhang, T. Peng, X. Nie, G.S. Agarwal, M.O. Scully, Entangled photons enabled time-frequency-resolved coherent Raman spectroscopy and applications to electronic coherences at femtosecond scale, Light.: Sci. Appl. 11 (1) (2022) 274.
[8] W. Chen, S. Qiao, Z. Lang, J. Jiang, Y. He, Y. Shi, Y. Ma, Hollow-waveguide-based light-induced thermoelastic spectroscopy sensing, Opt. Lett. 48 (15) (2023) 3989–3992.
[9] M. Yan, P.-L. Luo, K. Iwakuni, G. Millot, T.W. Hänsch, N. Picqué, Mid-infrared dual-comb spectroscopy with electro-optic modulators, Light.: Sci. Appl. 6 (10) (2017) e17076.
[10] Y. Ma, T. Liang, S. Qiao, X. Liu, Z. Lang, Highly Sensitive and fast hydrogen detection based on light-induced thermoelastic spectroscopy, Ultra Sci. 3 (2023) 0024.
[11] R. Cui, H. Wu, L. Dong, W. Chen, F.K. Tittel, Multiple-sound-source-excitation quartz-enhanced photoacoustic spectroscopy based on a single-line spot pattern multi-pass cell, Appl. Phys. Lett. 118 (16) (2021) 161101.
[12] Z. Gong, T. Gao, L. Mei, K. Chen, Y. Chen, B. Zhang, W. Peng, Q. Yu, Ppb-level detection of methane based on an optimized T-type photoacoustic cell and a NIR diode laser, Photoacoustics 21 (2021) 100216.
[13] Z. Lang, S. Qiao, Y. Ma, Fabry–Perot-based phase demodulation of heterodyne light-induced thermoelastic spectroscopy, Light.: Adv. Manuf. 4 (2) (2023) 1–10.
[14] C. Zhang, Y. He, S. Qiao, Y. Ma, Differential integrating sphere-based photoacoustic spectroscopy gas sensing, Opt. Lett. 48 (19) (2023) 5089–5092.
[15] C. Fang, S. Qiao, Y. He, Z. Shen, Y. Ma, Design and sensing performance of T-shaped quartz tuning forks, Acta Opt. Sin. 43 (18) (2023).
[16] Z. Gong, T. Gao, Y. Chen, B. Zhang, W. Peng, Q. Yu, F. Ma, L. Mei, K. Chen, Sub-ppb level detection of nitrogen dioxide based on an optimized H-type longitudinal acoustic resonator and a lock-in white-light interferometry demodulation algorithm, J. Quant. Spectrosc. Radiat. Transf. 253 (2020) 107136.
[17] A. Fathy, Y.M. Sabry, I.W. Hunter, D. Khalil, T. Bourouina, Direct absorption and photoacoustic spectroscopy for gas sensing and analysis: a critical review, Laser Photonics Rev. 16 (8) (2022) 2100556.
[18] L. Zhang, L. Liu, Y. Liu, X. Zhang, H. Huan, X. Yin, T. Xi, X. Shao, Advances in differential photoacoustic spectroscopy for trace gas detection, Microw. Opt. Technol. Lett. 65 (5) (2023) 1506–1515.
[19] A. Elia, C. Di Franco, P.M. Lugarà, G. Scamarcio, Photoacoustic spectroscopy with quantum cascade lasers for trace gas detection, Sensors 6 (10) (2006) 1411–1419.
[20] A. Sampaolo, P. Patimisco, M. Giglio, A. Zifarelli, H. Wu, L. Dong, V. Spagnolo, Quartz-enhanced photoacoustic spectroscopy for multi-gas detection: a review, Anal. Chim. Acta 1202 (2022) 338894.
[21] T. Yang, W. Chen, P. Wang, A review of all-optical photoacoustic spectroscopy as a gas sensing method, Appl. Spectrosc. Rev. 56 (2) (2021) 143–170.
[22] S. Qian, C. Tian, Z. Wang, Y. Yu, S. Bi, X. Zhang, Elimination of laser power loss influence for multi-point gas sensing in photoacoustic spectroscopy, IEEE Sens. J. 21 (9) (2021) 10571–10578.
[23] Z. Gong, G. Wu, X. Jiang, H. Li, T. Gao, M. Guo, F. Ma, K. Chen, L. Mei, W. Peng, All-optical high-sensitivity resonant photoacoustic sensor for remote CH_4 gas detection, Opt. Express 29 (9) (2021) 13600–13609.
[24] Y. Ma, Y. Hong, S. Qiao, Z. Lang, X. Liu, H-shaped acoustic micro-resonator-based quartz-enhanced photoacoustic spectroscopy, Opt. Lett. 47 (3) (2022) 601–604.
[25] K. Chen, R. An, C. Li, Y. Kang, F. Ma, X. Zhao, M. Guo, H. Qi, J. Zhao, Detection of ultra-low concentration acetylene gas dissolved in oil based on fiber-optic photoacoustic sensing, Opt. Laser Technol. 154 (2022) 108299.
[26] T. Yang, W. Chen, Z. Zhang, J. Lei, F. Wan, R. Song, Multiple reflections enhanced fiber-optic photoacoustic sensor for gas micro-leakage, Opt. Express 29 (2) (2021) 2142–2152.
[27] C. Zhang, Q. Wang, X. Yin, Photoacoustic spectroscopy for detection of trace C_2H_2 using ellipsoidal photoacoustic cell, Opt. Commun. 487 (2021) 126764.
[28] Y. Ma, S. Qiao, Y. He, Y. Li, Z. Zhang, X. Yu, F.K. Tittel, Highly sensitive acetylene detection based on multi-pass retro-reflection-cavity-enhanced photoacoustic spectroscopy and a fiber amplified diode laser, Opt. Express 27 (10) (2019) 14163–14172.
[29] C. Zhang, Q. Wang, H. Pan, F. Pian, Z. Li, P. Shan, Highly sensitive multi-pass enhanced photoacoustic cell based on three spot-ring structure (TSR-MPC), Infrared Phys. Technol. 118 (2021) 103880.
[30] H. Pan, Q. Wang, C. Zhang, Z. Li, P. Shan, Z. Ma, High-sensitivity acetylene detection system using ellipsoid multi-pass cell (EMPC) based on the opposite dual optical source, Infrared Phys. Technol. 118 (2021) 103874.
[31] M. Zhang, B. Zhang, K. Chen, M. Guo, S. Liu, Y. Chen, Z. Gong, Q. Yu, Z. Chen, M. Liao, Miniaturized multi-pass cell based photoacoustic gas sensor for parts-per-billion level acetylene detection, Sens. Actuators A: Phys. 308 (2020) 112013.
[32] S. Zha, L. Li, Q. Zhang, H. Ma, S. Zhan, Y. Li, C. Zha, Variable diameter T-shaped cell-based photoacoustic sensor for trace gas detection, Microw. Opt. Technol. Lett. 65 (5) (2023) 1223–1228.
[33] L. Liu, A. Mandelis, H. Huan, K. Michaelian, A. Melnikov, Step scan T-cell Fourier-transform infrared photoacoustic spectroscopy (FTIR-PAS) for detection of ambient air contaminants, Vib. Spectrosc. 87 (2016) 94–98.
[34] Z. Gong, K. Chen, Y. Chen, L. Mei, Q. Yu, Integration of T-type half-open photoacoustic cell and fiber-optic acoustic sensor for trace gas detection, Opt. Express 27 (13) (2019) 18222–18231.
[35] Y. Jiao, H. Fan, Z. Gong, K. Yang, F. Shen, K. Chen, L. Mei, W. Peng, Q. Yu, Trace CH_4 gas detection based on an integrated spherical photoacoustic cell, Appl. Sci. 11 (11) (2021) 4997.
[36] Q. Wang, X. Yin, L. Yang, L. Xing, Geometrical optimization of resonant ellipsoidal photoacoustic cell in photoacoustic spectroscopy system, Spectrosc. Spectr. Anal. 40 (5) (2020) 1351–1355.
[37] G. Cheng, Y. Cao, X. Tian, K. Liu, J. Cheng, Calculation and evaluation of acoustic and flow field characteristics of trapezoid compound photoacoustic cell, Acta Photon. Sin. 50 (2021) 0230001.
[38] W. Sun, S. Song, B. Qian, D. Wen, D. Jiang, Y. Fu, Q. Wang, Quantitative analysis of blood glucose by FT-Raman spectroscopy and multivariate statistical analysis, Microw. Opt. Technol. Lett. (2023) 1–7.
[39] O. Devos, L. Duponchel, Parallel genetic algorithm co-optimization of spectral pre-processing and wavelength selection for PLS regression, Chemom. Intell. Lab. Syst. 107 (1) (2011) 50–58.
[40] Q. Wang, S. Song, L. Li, D. Wen, P. Shan, Z. Li, Y. Fu, An extreme learning machine optimized by differential evolution and artificial bee colony for predicting the concentration of whole blood with Fourier Transform Raman spectroscopy, 292 (2023) 122423.
[41] F. Pian, Q. Wang, M. Wang, P. Shan, Z. Li, Z. Ma, A shallow convolutional neural network with elastic nets for blood glucose quantitative analysis using Raman spectroscopy, Spectrochim. Acta Part A: Mol. Biomol. Spectrosc. 264 (2022) 120229.
[42] Q. Wang, G. Wu, F. Pian, P. Shan, Z. Li, Z. Ma, Simultaneous detection of glucose, triglycerides, and total cholesterol in whole blood by Fourier-Transform Raman spectroscopy, Spectrochim. Acta Part A: Mol. Biomol. Spectrosc. 260 (2021) 119906.
[43] C. De Bleye, P.F. Chavez, J. Mantanus, R. Marini, P. Hubert, E. Rozet, E. Ziemons, Critical review of near-infrared spectroscopic methods validations in pharmaceutical applications, J. Pharm. Biomed. Anal. 69 (2012) 125–132.
[44] N. V.R, A.K. Mohapatra, R. Nayak, U. V.K, V.B. Kartha, S. Chidangil, UV laser-based photoacoustic breath analysis for the diagnosis of respiratory diseases: Detection of Asthma, Sens. Actuators B: Chem. 370 (2022).
[45] A. Shrivastava, V.B. Gupta, Methods for the determination of limit of detection and limit of quantitation of the analytical methods, Chron. Young-.-. Sci. 2 (1) (2011) 21–25.
[46] M. Blanco, M. Castillo, A. Peinado, R. Beneyto, Determination of low analyte concentrations by near-infrared spectroscopy: effect of spectral pretreatments and estimation of multivariate detection limits, Anal. Chim. Acta 581 (2) (2007) 318–323.
[47] M. Guo, K. Chen, B. Yang, C. Li, B. Zhang, Y. Yang, Y. Wang, C. Li, Z. Gong, F. Ma, Ultrahigh sensitivity fiber-optic Fabry–Perot interferometric acoustic sensor based on silicon cantilever, IEEE Trans. Instrum. Meas. 70 (2021) 1–8.

Qiaoyun Wang received the B.S. degree from Tangshan Normal University in 2003, and the Ph.D. degree in Optical Engineering from the Dalian University of Technology in 2010. Dr. Wang is now an associate professor in the School of Control Engineering at Northeastern University at Qinhuangdao. Her research interests include photoacoustic spectroscopy, fiber optical sensors, infrared spectroscopy, Raman spectroscopy and acoustofluidic, and their applications.

Shunyuan Xu received his B.S. degree in Yancheng Institute of Technology, China, in 2018. He is now pursuing a master's degree in control engineering from Northeastern University. His research interest is photoacoustic cell design based on photoacoustic spectroscopy.

Ziheng Zhu received his B.S. degree in China Jiliang University, China, in 2023. He is now pursuing a master's degree of optical engineering from Northeastern University. His research interest is photoacoustic cell design based on photoacoustic spectroscopy.

Jilong Wang received his B.S. degree in Qingdao University of Technology, China, in 2018. He is now pursuing a master's degree in control engineering from Northeastern University. His research interest is fiber optic Fabry-Perot micro pressure sensor.

Xin Zou received her B.S. degree in East China Jiaotong University, China, in 2018. He is now pursuing a master's degree of Control Science and Engineering from Northeastern University. His research interest is research on spectral quantitative analysis algorithm.

Chu Zhang received her B.S. degree in Qingdao University of Technology, China, in 2019. Then, she obtained a master's degree in control engineering from Northeastern University. She is now pursuing a PhD degree of physical electronics from Harbin Institute of Technology. Her research interest is photoacoustic cell design based on photoacoustic spectroscopy.

Qiang Liu received the B.S. and Ph.D. degrees from the College of Science, Yanshan University, Qinhuangdao, China, in 2013 and 2018, respectively. He is an Assistant Professor with the School of Control Engineering at Northeastern University at Qinhuangdao. He has authored and coauthored more than 50 scientific articles. His research interests include fiber optical sensors, fiber modulators, polarization filters, fiber splitters, functional materials, smart materials, photonic crystal fibers, and their applications.